國立臺灣大學工學院化學工程學系

碩士論文

Department of Chemical Engineering

College of Engineering

National Taiwan University

Master's Thesis

球形複合粒子平行單一或兩平板之緩慢移動與轉動

Slow Translation and Rotation of a Composite Sphere Parallel to One or Two Planar Walls

周郁富

Yu-Fu Chou

指 導 教 授 ： 葛煥彰 教授

Advisor: Huan-Jang Keh, Professor

中華民國 一百一十四 年 七 月

July, 2025

doi:10.6342/NTU202502370

謝辭

能夠順利完成這篇論文，首先我要感謝我的指導老師 葛煥彰教授。感謝老師在我就學期間指引我正確的研究方向並時時刻刻督促我認真做研究，每當研究遇到瓶頸時，老師不會對我有過多的苛責，反而會選擇相信我的能力，給我時間解決複雜有挑戰性的問題，讓我一一克服困難並完成此篇論文。老師除了擁有清晰的邏輯和淵博的專業知識外，還有非常嚴謹的研究態度，這些不僅讓我在學習上受益良多，也讓我在做事態度和面對研究上成長許多，在此由衷感謝老師這兩年來的細心指導。同時也感謝兩位口試委員 詹正雄教授與謝子賢博士，謝謝他們撥冗審核我的論文，並在口試時給予寶貴的建議，使得本論文更趨於完善。

再來，我要感謝實驗室的學長姊、同學以及學弟們。感謝旻叡學長，雖然與他相處只有不到兩個月，但他卻不厭其煩地教會了我許多研究方面的技能並提供他的寶貴經驗，使我在推導數學式子及程式上更快上手。感謝家菶學姊、展維學長和永捷學長在我碩一那年帶領我熟悉實驗室以及碩班的生活，並在研究和實驗室會議給我許多建議。感謝同學亦銓和威鋅在課業討論、研究都給我許多幫助，你們都很優秀，讓我在研究和課業上如虎添翼。感謝學弟陳沂和威齊，你們認真做研究並幫忙了許多實驗室的事情，祝你們都能順利畢業。

最後，我要感謝我的家人，謝謝父母從小到大的栽培，並且無條件地支持我，讓我能無後顧之憂地完成我的碩士學位。

民國 一百一十四年 七月

周郁富

doi:10.6342/NTU202502370

摘要

本論文以半解析的方式探討一個球形複合粒子(構造為一個流體不可滲透的硬質核心固體，外圍包覆著一層流體可滲透的多孔物質)在黏性流體中，平行於一個或兩個平板邊界，所進行的穩態低雷諾數耦合移動與轉動。多孔層內外之流體速度分別由 Brinkman 方程式及 Stokes 方程式主導。研究中，分別利用球坐標與直角坐標下的基本解建立通解。首先代入平板的邊界條件並透過傅立葉轉換法解析求解，接著代入多孔層內外球面的邊界條件並使用邊界取點法數值計算，獲得流體施加於粒子之拖曳力與力矩。數值計算顯示，在廣泛的物理參數範圍內，所得的阻力與力矩均具有良好的收斂性。為驗證數據合理性，針對不可滲透硬質固體球平行於單一或兩平板的結果，與既有文獻中的對應結果進行比對，吻合良好。流體施加於複合粒子的拖曳力與力矩隨著粒子半徑與流體於多孔層穿透長度之比值、固體核半徑與粒子半徑之比值、粒子半徑與較近平板間距之比值增加而單調遞增。結果亦發現，平板對粒子移動的影響明顯大於對其轉動的影響。比較平行於平板與垂直於平板的運動時，平面邊界在粒子平行運動時對粒子產生的流體拖曳力較小，但所施加的力矩則較大。此外，複合球在平行於平板運動時，移動與轉動的耦合作用表現出複雜的行為，其變化並不隨系統參數的改變而單調變化。

關鍵詞：複合粒子、多孔球、拖曳力與力矩、蠕動流、平板邊界效應

doi:10.6342/NTU202502370

Abstract

A semi-analytical investigation is conducted to examine the coupled translational and rotational motions of a composite spherical particle (consisting of an impermeable hard core surrounded by a permeable porous shell) immersed in a viscous fluid parallel to one or two planar boundaries under the steady condition of a low Reynolds number. The fluid flow is described using the Stokes equations outside the porous shell and the Brinkman equation within it. A general solution is formulated by employing fundamental solutions in both spherical and Cartesian coordinate systems. The boundary conditions on the planar walls are implemented using the Fourier transform method, while those on the inner and outer boundaries of the porous shell are applied via a collocation technique. Numerical calculations yield hydrodynamic force and torque results with good convergence across a broad range of physical parameters. For validation, the results corresponding to an impermeable hard sphere parallel to one or two planar walls are shown to be in close agreement with established solutions from the literature. The hydrodynamic drag force and torque experienced by the composite particle increase steadily with larger values of the ratio of the particle radius to the porous shell's permeation length, the ratio of the core radius to the total particle radius, and the

doi:10.6342/NTU202502370

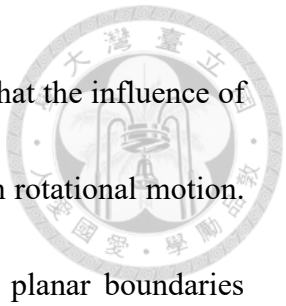

separations between the particle and the walls. It has been observed that the influence of the walls on translational motion is significantly stronger than that on rotational motion. When comparing motions parallel versus normal to the walls, the planar boundaries impose weaker hydrodynamic forces but stronger torques during parallel motions. The coupling between the translation and rotation of the composite sphere parallel to the walls exhibits complex behavior that does not vary monotonically with changes in system parameters.

Keywords: composite particle; porous sphere; drag force and torque; creeping flow; boundary effect in slit

doi:10.6342/NTU202502370

Table of Contents

doi:10.6342/NTU202502370

doi:10.6342/NTU202502370

List of Figures

doi:10.6342/NTU202502370

doi:10.6342/NTU202502370

List of Tables

doi:10.6342/NTU202502370

Chapter 1
Introduction

The motion of small particles in viscous fluids, including their translation and rotation at low Reynolds numbers, continues to attract significant attention from researchers in various scientific, technological, and engineering domains. These fundamental processes provide a deep understanding of many practical systems, such as sedimentation, centrifugation, coagulation, filtration, aerosol technologies, suspension rheology, microfluidics, electrophoresis, and other phoretic movements. Stokes was the first to analyze the creeping motions of a hard, impermeable sphere in an unbounded Newtonian fluid [1,2], and these works were later expanded to cover the translation and rotation of a composite sphere [3,4].

A composite sphere, with a radius b, consists of a hard sphere core of radius a, which is surrounded by a permeable porous layer of thickness $b-a$. Typical examples of composite particles include biological cells with rough surface structures, ranging from micrometer-sized cilia to nanometer-sized protein molecules [5], as well as polystyrene latex particles with a porous surface extending into the surrounding fluid [6]. Colloidal suspension particles can be sterically stabilized against aggregation by purposely adsorbing polymers and forming porous surface layers [7].

doi:10.6342/NTU202502370

When a composite particle of radius b, with a hard core of radius a, translates with velocity $\mathbf{U}$ and rotates with angular velocity $\mathbf{\Omega}$ in an unbounded fluid of viscosity η, the hydrodynamic force and torque acting on the particle are [3,4]

$$\begin{aligned}\mathbf{F}_0 = -6\pi\eta\lambda^{-1}\{&W\lambda a\cosh\lambda a - 3\lambda^2a^2(V+\lambda a\sinh\lambda a)+[(\lambda aV-\lambda b\cosh\lambda a)W\\ &+3\lambda^3a^2b\sinh\lambda a]G_1+[W\cosh\lambda a+3\lambda^2a^2(\lambda aV-\sinh\lambda a)]G_2\}\\ &\times\{(\lambda a\sinh\lambda b-\cosh\lambda a)[(W+3\lambda b)G_1+3(\lambda^2a^2-1)G_2-6\lambda a]\}^{-1}\mathbf{U},\end{aligned} \tag{1}$$

$$\mathbf{T}_0 = -8\pi\eta b^3\left[1+\frac{3}{\lambda^2b^2}-\frac{3(G_1+\lambda aG_2)}{\lambda b(G_2+\lambda aG_1)}\right]\mathbf{\Omega}, \tag{2}$$

where

$$G_1=\cosh(\lambda b-\lambda a), \qquad G_2=\sinh(\lambda b-\lambda a), \tag{3}$$

$$V=\lambda b\sinh\lambda b-\cosh\lambda b, \qquad W=2\lambda^3b^3+\lambda^3a^3+3\lambda a, \tag{4}$$

and λ^{-1} is the square root of the fluid permeability or flow penetration length within the porous surface layer of the particle. The drag force and torque exerted on the particle are proportional to the translational and angular velocities, respectively. Note that the translation and rotation are uncoupled in the case of an unconfined composite sphere; i.e., $\mathbf{F}_0$ and $\mathbf{T}_0$ are independent of $\mathbf{\Omega}$ and $\mathbf{U}$, respectively. In the limiting cases where $a=b$ and $a=0$, Equations (1) and (2) reduce to the Stokes results ($\mathbf{F}_0=-6\pi\eta b\mathbf{U}$ and $\mathbf{T}_0=-8\pi\eta b^3\mathbf{\Omega}$) for a hard sphere and equivalent results for a completely porous (permeable) sphere [4,8], respectively, of radius b. In the limits $\lambda b=0$ and $\lambda b\to\infty$, these equations simplify to the Stokes results for a hard sphere with radii a and b,

doi:10.6342/NTU202502370

respectively. Note that $(\lambda b)^{-2}$ is known as the Darcy number.

In real-world scenarios, particles are not isolated, and the surrounding fluid is constrained by solid boundaries [9-11]. Therefore, it is crucial to determine whether the proximity of a boundary significantly influences the motion of the particles. Past research has extensively analyzed the low-Reynolds-number translation and rotation of a hard sphere near various types of boundaries [12-21]. Additionally, studies have also investigated the slow translation and rotation of a composite sphere inside a concentric [4,22,23] or non-concentric [24-26] spherical cavity, within a circular cylinder [27], and perpendicular to one or two planar walls [28,29]. These studies demonstrate that boundary effects on the motion of both hard and composite particles can be significant and intriguing.

In practical applications, we often encounter translations and rotations of a composite sphere near one or two planar walls but not perpendicular to the walls. The aim of this thesis is to derive a semi-analytical solution for the slow translation and rotation of a composite sphere parallel to one or two planar walls. These parallel motions present more complex challenges because they break the azimuthal symmetry, causing the translation and rotation to become coupled. By combining analytical and numerical techniques, the Stokes and Brinkman equations governing the external and internal fluid flows, respectively, with respect to the porous layer are solved using a boundary

doi:10.6342/NTU202502370

collocation approach. The wall-corrected drag force and torque exerted by the fluid on the composite particle are then determined, with the solutions showing good convergence. Since the problem of slow translation and rotation of a composite sphere in arbitrary directions near one or two large planar walls is linear, the solutions can be obtained by superimposing the solutions to two subproblems: motions normal to the planar walls, which have been previously studied [28,29], and motions parallel to the planar walls, which are addressed in this thesis.

doi:10.6342/NTU202502370

Chapter 2

Analysis

As shown in Figure 1, we consider the steady motion of a viscous fluid caused by a composite particle of radius b, consisting of a hard sphere core of radius a and a porous surface layer of thickness $b-a$, translating with velocity $\mathbf{U}=U\mathbf{e}_x$ and rotating with angular velocity $\mathbf{\Omega}=\Omega\mathbf{e}_y$ parallel to two large stationary planar walls (both normal to $\mathbf{e}_z$) at distances c and d from the center of the composite sphere. Here, (x,y,z), (ρ,ϕ,z), and (r,θ,ϕ) represent the Cartesian, cylindrical, and spherical coordinate systems, respectively, originating from the particle center, $\mathbf{e}_x$, $\mathbf{e}_y$, and $\mathbf{e}_z$ are the principal unit vectors in the Cartesian coordinates, and $\mathbf{e}_r$, $\mathbf{e}_\theta$, and $\mathbf{e}_\phi$ are the principal unit vectors in the spherical coordinates. We set $d \le c$ throughout the article without loss of generality. The fluid is at rest away from the composite sphere and on the nonslip planar walls. Our aim is to determine the modification of Equations (1) and (2) for the translational and rotational motions of a composite sphere due to the presence of the planar walls.

doi:10.6342/NTU202502370

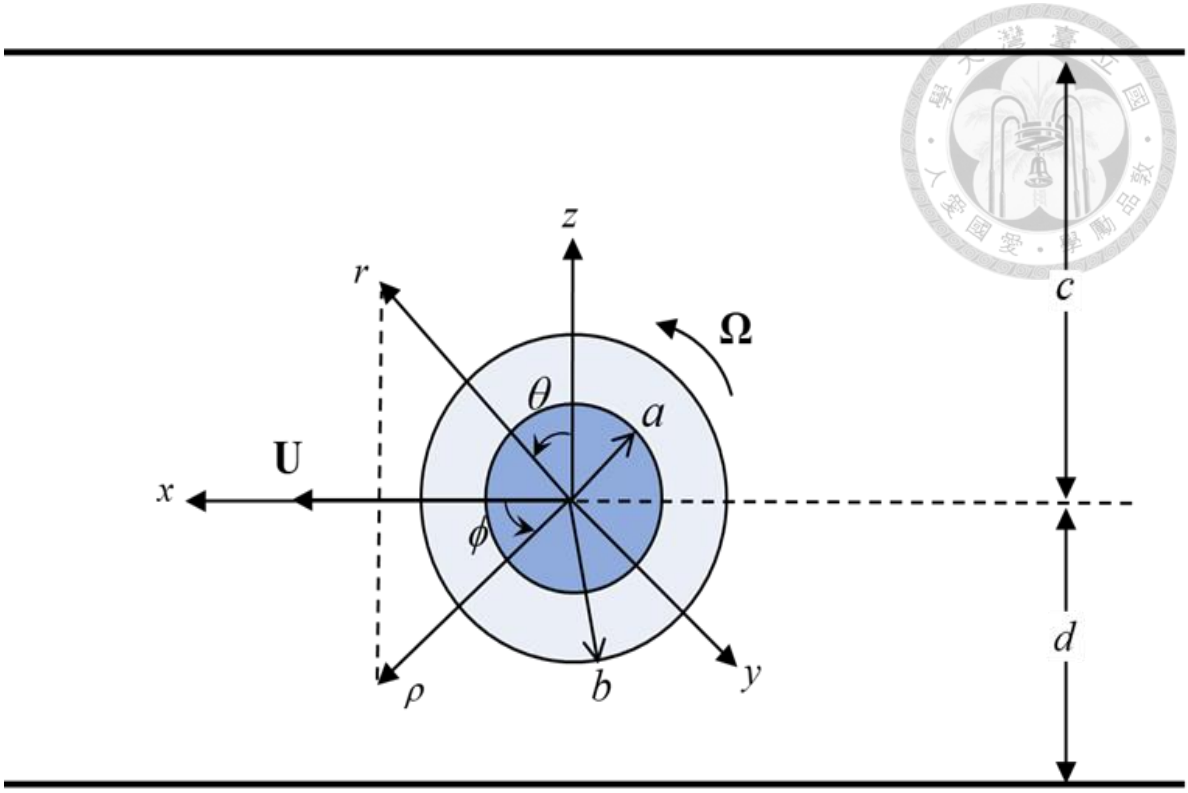

Figure 1. Schematic illustration of the translation and rotation of a composite sphere parallel to two plane walls at an arbitrary position between them.

doi:10.6342/NTU202502370

2.1. Governing equations and boundary conditions

For the creeping flow of an incompressible Newtonian fluid, the fluid velocity, $\mathbf{v}$, and pressure, p, outside the composite sphere are governed by the Stokes equations, as follows:

$$\eta\nabla^2\mathbf{v}-\nabla p=\mathbf{0},\qquad \nabla\cdot\mathbf{v}=0\qquad\qquad (r\geq b), \tag{5}$$

where η is the fluid viscosity. Within the porous surface layer, the Brinkman and continuity equations,

$$\eta\nabla^2\hat{\mathbf{v}}-\nabla\hat{p}-\eta\lambda^2(\hat{\mathbf{v}}-\mathbf{U}-\boldsymbol{\Omega}\times\mathbf{r})=\mathbf{0},\qquad \nabla\cdot\hat{\mathbf{v}}=0\qquad (a\leq r\leq b), \tag{6}$$

are used to govern the fluid velocity, $\hat{\mathbf{v}}$, and pressure, $\hat{p}$, where the effective viscosity of the fluid is assumed to equal the viscosity of the bulk fluid [3,28,30], λ^2 is the reciprocal of permeability, and $\mathbf{r}=r\mathbf{e}_r$ is the position vector.

The boundary conditions for the external and internal fluid flows are

$$r=a:\qquad \hat{\mathbf{v}}=\mathbf{U}+a\boldsymbol{\Omega}\times\mathbf{e}_r, \tag{7}$$

$$r=b:\qquad \mathbf{v}=\hat{\mathbf{v}}, \tag{8a}$$

$$\mathbf{e}_r\cdot(\boldsymbol{\tau}-p\mathbf{I})=\mathbf{e}_r\cdot(\hat{\boldsymbol{\tau}}-\hat{p}\mathbf{I}), \tag{8b}$$

$$z=c,-d:\qquad \mathbf{v}=\mathbf{0}, \tag{9}$$

$$\rho\to\infty:\quad \mathbf{v}=\mathbf{0}, \tag{10}$$

where $\boldsymbol{\tau}$ and $\hat{\boldsymbol{\tau}}$ are viscous stress tensors for the external and internal flows, respectively, and $\mathbf{I}$ is the unit tensor. It can be shown that the boundary condition in

doi:10.6342/NTU202502370

Equation (8b), which represents the continuity of the total stress on the outer surface of the porous layer, is equivalent to

$$r = b: \qquad p = \hat{p}, \quad \frac{\partial v_\theta}{\partial r} = \frac{\partial \hat{v}_\theta}{\partial r}, \quad \frac{\partial v_\phi}{\partial r} = \frac{\partial \hat{v}_\phi}{\partial r}, \tag{11}$$

where $(v_\theta, \hat{v}_\theta)$ and $(v_\phi, \hat{v}_\phi)$ are θ and ϕ components of the relevant fluid velocities, respectively.

doi:10.6342/NTU202502370

2.2. Solution for the fluid velocity and pressure

A general solution of the external fluid velocity that satisfies Equations (5), (9), and (10) is

$$\mathbf{v} = v_x \mathbf{e}_x + v_y \mathbf{e}_y + v_z \mathbf{e}_z , \tag{12}$$

where

$$v_x = \sum_{n=1}^{\infty} [A_n (A_n' + \alpha_n') + B_n (B_n' + \beta_n') + C_n (C_n' + \gamma_n')], \tag{13a}$$

$$v_y = \sum_{n=1}^{\infty} [A_n (A_n'' + \alpha_n'') + B_n (B_n'' + \beta_n'') + C_n (C_n'' + \gamma_n'')], \tag{13b}$$

$$v_z = \sum_{n=1}^{\infty} [A_n (A_n''' + \alpha_n''') + B_n (B_n''' + \beta_n''') + C_n (C_n''' + \gamma_n''')], \tag{13c}$$

the primed A_n, B_n, C_n, α_n, β_n, and γ_n are functions of position defined by Equations (2.6) and (C1) of Ganatos et al. [13], and A_n, B_n, and C_n are unknown constants. The corresponding solution for the fluid pressure can be obtained by integrating Equation (5a) with the following result:

$$p = \eta \sum_{n=1}^{\infty} [A_n A_n'''' + B_n B_n'''' + C_n C_n''''], \tag{14}$$

where A_n'''', B_n'''', and C_n'''' are functions of position, which are lengthy and defined by Equations (A10)–(A12) in Appendix A. All numerical integrations used to evaluate the primed A_n, B_n, C_n, α_n, β_n, and γ_n functions are performed using the Gauss–Laguerre quadrature method.

doi:10.6342/NTU202502370

The general solution of the internal fluid velocity satisfying Equation (6) can be obtained as

$$\hat{\mathbf{v}} = \hat{v}_r \mathbf{e}_r + \hat{v}_\theta \mathbf{e}_\theta + \hat{v}_\phi \mathbf{e}_\phi , \tag{15}$$

where

$$\hat{v}_r = [\sum_{n=1}^{\infty} n(n+1) P_n^1(\mu)\{\hat{C}_{1n} r^{n-1} + \hat{C}_{2n} r^{-n-2} + r^{-3/2}[\hat{C}_{3n} I_{n+1/2}(\lambda r) + \hat{C}_{4n} K_{n+1/2}(\lambda r)]\} + U(1-\mu^2)^{1/2}]\cos\phi , \tag{16a}$$

$$\hat{v}_\theta = [\sum_{n=1}^{\infty} \{[-\hat{C}_{1n}(n+1) r^{n-1} + n\hat{C}_{2n} r^{-n-2} + \hat{C}_{3n}\{n r^{-3/2} I_{n+1/2}(\lambda r) - \lambda r^{-1/2} I_{n-1/2}(\lambda r)\} + \hat{C}_{4n}\{n r^{-3/2} K_{n+1/2}(\lambda r) + \lambda r^{-1/2} K_{n-1/2}(\lambda r)\}](1-\mu^2)^{1/2} \frac{dP_n^1(\mu)}{d\mu} + r^{-1/2}[\hat{D}_{1n} I_{n+1/2}(\lambda r) + \hat{D}_{2n} K_{n+1/2}(\lambda r)](1-\mu^2)^{-1/2} P_n^1(\mu)\} + U\mu + \Omega r]\cos\phi , \tag{16b}$$

$$\hat{v}_\phi = [\sum_{n=1}^{\infty} \{[-\hat{C}_{1n}(n+1) r^{n-1} + n\hat{C}_{2n} r^{-n-2} + \hat{C}_{3n}\{n r^{-3/2} I_{n+1/2}(\lambda r) - \lambda r^{-1/2} I_{n-1/2}(\lambda r)\} + \hat{C}_{4n}\{n r^{-3/2} K_{n+1/2}(\lambda r) + \lambda r^{-1/2} K_{n-1/2}(\lambda r)\}](1-\mu^2)^{-1/2} P_n^1(\mu) + r^{-1/2}[\hat{D}_{1n} I_{n+1/2}(\lambda r) + \hat{D}_{2n} K_{n+1/2}(\lambda r)](1-\mu^2)^{1/2} \frac{dP_n^1(\mu)}{d\mu}\} - U - \Omega r\mu]\sin\phi , \tag{16c}$$

$\mu = \cos\theta$, I_n and K_n are the modified Bessel function of the first and second kinds of order *n*, respectively, P_n^1 is the associated Legendre function of order *n* and degree one, and $\hat{C}_{1n}$, $\hat{C}_{2n}$, $\hat{C}_{3n}$, $\hat{C}_{4n}$, $\hat{D}_{1n}$, and $\hat{D}_{2n}$ are unknown constants. Similar to the derivation of the external fluid pressure, the integration of Equation (6a) yields the internal fluid pressure as follows:

$$\hat{p} = -\eta\lambda^2 \cos\phi \sum_{n=1}^{\infty} [(n+1)\hat{C}_{1n} r^n - n\hat{C}_{2n} r^{-n-1}] P_n^1(\mu) . \tag{17}$$

doi:10.6342/NTU202502370

The boundary conditions that still need to be satisfied are the conditions of the inner and outer surfaces of the porous layer of the composite sphere. By substituting Equations (12)–(17) into Equations (7) and (8), we obtain simultaneous linear algebraic Equations (A1)–(A9), which are lengthy, in Appendix A. The unknown constants A_n, B_n, C_n, $\hat{C}_{1n}$, $\hat{C}_{2n}$, $\hat{C}_{3n}$, $\hat{C}_{4n}$, $\hat{D}_{1n}$, and $\hat{D}_{2n}$ will be determined using these lengthy equations.

A careful inspection of Equations (A1)–(A9) shows that the solution to the resulting unknown constant matrix is independent of the coordinate, ϕ, of the boundary points on spheres $r = a$ and $r = b$. If the infinite series in Equations (13), (14), (16), and (17) are truncated after *N* terms and then the truncated form of Equations (A1)–(A9) are satisfied at *N* discrete points on the half-circular generating arc of each spherical surface (from $\theta = 0$ to $\theta = \pi$), the resulting system of 9*N* simultaneous linear algebraic equations can be solved numerically to yield the 9*N* unknown constants, A_n, B_n, C_n, $\hat{C}_{1n}$, $\hat{C}_{2n}$, $\hat{C}_{3n}$, $\hat{C}_{4n}$, $\hat{D}_{1n}$, and $\hat{D}_{2n}$, that appear in the truncated form of Equations (13), (14), (16), and (17). The accuracy of the fluid velocity and pressure solutions obtained using this boundary collocation method can reach the required level as long as the *N* value is large enough.

doi:10.6342/NTU202502370

2.3. Hydrodynamic force and torque on the composite particle

The drag force, $\mathbf{F} = F\mathbf{e}_x$, and torque, $\mathbf{T} = T\mathbf{e}_y$, exerted on the composite sphere by the fluid can be determined using [13]

$$F = -8\pi\eta A_1, \tag{18a}$$

$$T = -8\pi\eta C_1, \tag{18b}$$

in which only the unknown constants, A_1 and C_1, are needed. When $b/d = 0$, the planar walls are away from the composite sphere, and Equation (18a,b) for F and T become Equations (1) and (2) for F_0 and T_0 of an isolated particle, respectively.

The force, F, and torque, T, can also be related to the migration velocity, U, and angular velocity, Ω, of the confined particle using

$$F = \frac{F_0}{U}(F_{\mathrm{t}}U + F_{\mathrm{r}}b\Omega), \tag{19a}$$

$$T = \frac{T_0}{b\Omega}(T_{\mathrm{t}}U + T_{\mathrm{r}}b\Omega), \tag{19b}$$

where F_{t}, F_{r}, T_{t}, and T_{r} are the dimensionless resistance coefficients. According to the cross-effect theory of the force and torque on a spherical particle near boundaries, the coupling coefficients, F_{r} and T_{t}, are related using [12]

$$T_{\mathrm{t}} = \frac{F_0/U}{T_0/b^2\Omega}F_{\mathrm{r}}. \tag{20}$$

Therefore, only the solutions of the three coefficients, F_{t}, T_{r}, and F_{r}, need to be presented.

doi:10.6342/NTU202502370

Chapter 3

Results and Discussion

The boundary collocation solutions of the force, torque, and coupling coefficients, F_t, T_r, and F_r, respectively, in Equation (19) for the slow translation and rotation of a composite sphere parallel to two planar walls (convergent to the significant figures as given) for various values of the particle–wall spacing parameter, b/d, relative particle position parameter, $d/(d+c)$, core-to-particle radius ratio, a/b, and ratio of the particle radius to the porous layer permeation length, λb, are presented in Tables 1–3 for the special case of a porous sphere ($a=0$) and in Table 4 for the general case of a composite sphere. The geometric meanings of the aforementioned four parameters are depicted in Figure A1. Within the limit of $\lambda b \to \infty$ (the porous surface layer is impermeable), our numerical results are in good agreement with the corresponding collocation solutions obtained previously [14] for the translation and rotation of a hard sphere of radius, b, parallel to two planar walls. The wall effects on the translation and rotation of the composite particle can be significant. Note that the value of $d/(d+c)$ that is equal to 0 and 1/2 represents the cases of a particle translating and rotating parallel

doi:10.6342/NTU202502370

to a single planar wall and to two equally distant planar walls, respectively. Consistent with Equations (1) and (2), $F_r = T_t = 0$ (no coupling between translation and rotation of the composite sphere) and $F_t = T_r = 1$ at $b/d = 0$ (i.e., for an unconfined composite sphere) for any values of λb and a/b. Both F_t and T_r are greater than unity as long as b/d is finite (greater than zero) due to the hydrodynamic hindrance to the particle motions produced by the planar walls. Interestingly, the coupling coefficient, F_r, can be positive or negative depending on the values of the dimensionless parameters, b/d, $d/(d+c)$, a/b, and λb, as shown in Tables 3 and 4. This feature also appears in the translation and rotation of a hard sphere parallel to two planar walls [14]. Evidently, $F_r = T_t = 0$ for the symmetric case of $d/(d+c) = 1/2$ (two equally distant planar walls).

doi:10.6342/NTU202502370

Table 1. Force coefficient, F_t, for the translation of a porous sphere parallel to two planar walls at various values of $d/(d+c)$, b/d, and λb.

$d/(d+c)$	b/d	F_t				
		$\lambda b=1$	$\lambda b=10$	$\lambda b=100$	$\lambda b=300$	$\lambda b\to\infty$
0	0.1	1.0100	1.0525	1.0588	1.0593	1.0595
	0.2	1.0200	1.1103	1.1244	1.1254	1.1259
	0.3	1.0302	1.1740	1.1979	1.1995	1.2003
	0.4	1.0403	1.2448	1.2810	1.2835	1.2847
	0.5	1.0503	1.3243	1.3773	1.3810	1.3828
	0.6	1.0602	1.4154	1.4926	1.4980	1.5006
	0.7	1.0700	1.5225	1.6380	1.6463	1.6503
	0.8	1.0797	1.6531	1.8381	1.8522	1.8591
	0.9	1.0893	1.8219	2.1672	2.1995	2.2152
	0.99	1.0980	2.0377	2.9709	3.2285	3.3975
	0.999	1.0988	2.0656	3.2048	3.6843	4.1929
0.25	0.1	1.0116	1.0614	1.0689	1.0694	1.0697
	0.2	1.0233	1.1302	1.1471	1.1483	1.1489
	0.3	1.0352	1.2071	1.2361	1.2381	1.2391
	0.4	1.0470	1.2936	1.3382	1.3412	1.3427
	0.5	1.0588	1.3916	1.4568	1.4613	1.4635
	0.6	1.0704	1.5039	1.5983	1.6048	1.6080
	0.7	1.0818	1.6351	1.7738	1.7836	1.7884
	0.8	1.0931	1.7927	2.0082	2.0243	2.0322
	0.9	1.1042	1.9912	2.3759	2.4109	2.4279
	0.99	1.1142	2.2359	3.2183	3.4792	3.6724
	0.999	1.1152	2.2668	3.4570	3.9392	4.4494
0.5	0.1	1.0179	1.0975	1.1099	1.1107	1.1111
	0.2	1.0362	1.2134	1.2432	1.2452	1.2462
	0.3	1.0545	1.3504	1.4041	1.4078	1.4096
	0.4	1.0727	1.5114	1.5980	1.6039	1.6068
	0.5	1.0904	1.7002	1.8324	1.8413	1.8458
	0.6	1.1074	1.9222	2.1194	2.1329	2.1395
	0.7	1.1236	2.1854	2.4818	2.5024	2.5124
	0.8	1.1387	2.5033	2.9690	3.0029	3.0194
	0.9	1.1530	2.9019	3.7294	3.8019	3.8369
	0.99	1.1652	3.3877	5.4403	5.9675	6.2597
	0.999	1.1664	3.4488	5.9201	6.8900	7.6253

doi:10.6342/NTU202502370

Table 2. Torque coefficient, T_r, for the rotation of a porous sphere parallel to two planar walls at various values of $d/(d+c)$, b/d, and λb.

$d/(d+c)$	b/d	T_r				
		$\lambda b=1$	$\lambda b=10$	$\lambda b=100$	$\lambda b=300$	$\lambda b\to\infty$
0	0.1	1.0000	1.0002	1.0003	1.0003	1.0003
	0.2	1.0002	1.0018	1.0024	1.0025	1.0025
	0.3	1.0005	1.0062	1.0083	1.0085	1.0086
	0.4	1.0012	1.0149	1.0200	1.0205	1.0207
	0.5	1.0024	1.0299	1.0405	1.0413	1.0418
	0.6	1.0041	1.0536	1.0737	1.0754	1.0763
	0.7	1.0066	1.0899	1.1274	1.1307	1.1324
	0.8	1.0099	1.1457	1.2182	1.2249	1.2283
	0.9	1.0142	1.2352	1.3980	1.4161	1.4253
	0.99	1.0190	1.3768	1.9369	2.1072	2.2233
	0.999	1.0195	1.3974	2.1150	2.4519	2.8341
0.25	0.1	1.0000	1.0002	1.0003	1.0003	1.0003
	0.2	1.0002	1.0019	1.0025	1.0026	1.0026
	0.3	1.0005	1.0065	1.0086	1.0088	1.0089
	0.4	1.0013	1.0155	1.0208	1.0213	1.0215
	0.5	1.0025	1.0310	1.0420	1.0429	1.0433
	0.6	1.0043	1.0555	1.0763	1.0781	1.0789
	0.7	1.0068	1.0929	1.1314	1.1348	1.1365
	0.8	1.0103	1.1502	1.2241	1.2309	1.2344
	0.9	1.0147	1.2415	1.4062	1.4244	1.4337
	0.99	1.0197	1.3850	1.9476	2.1182	2.2463
	0.999	1.0203	1.4057	2.1262	2.4631	2.8455
0.5	0.1	1.0000	1.0004	1.0005	1.0005	1.0005
	0.2	1.0003	1.0031	1.0042	1.0043	1.0043
	0.3	1.0009	1.0107	1.0143	1.0146	1.0147
	0.4	1.0021	1.0258	1.0347	1.0354	1.0358
	0.5	1.0041	1.0519	1.0707	1.0722	1.0730
	0.6	1.0071	1.0940	1.1304	1.1335	1.1351
	0.7	1.0113	1.1598	1.2289	1.2350	1.2381
	0.8	1.0170	1.2629	1.3996	1.4123	1.4188
	0.9	1.0243	1.4318	1.7463	1.7815	1.7994
	0.99	1.0327	1.7046	2.8108	3.1503	3.3477
	0.999	1.0336	1.7446	3.1658	3.8382	4.3955

doi:10.6342/NTU202502370

Table 3. Coupling coefficient, $F_r = T_t(T_0 / b^2\Omega) / (F_0 / U)$, for the translation and rotation of a porous sphere parallel to two planar walls at various values of $d/(d+c)$, b/d, and λb.

$d/(d+c)$	b/d	F_r				
		$\lambda b = 1$	$\lambda b = 10$	$\lambda b = 100$	$\lambda b = 300$	$\lambda b \to \infty$
0	0.1	-4.7×10^{-7}	-7.4×10^{-6}	-1.1×10^{-5}	-1.2×10^{-5}	-1.2×10^{-5}
	0.2	-7.5×10^{-6}	-1.2×10^{-4}	-1.8×10^{-4}	-1.8×10^{-4}	-1.8×10^{-4}
	0.3	-3.8×10^{-5}	-5.7×10^{-4}	-8.6×10^{-4}	-8.9×10^{-4}	-9.0×10^{-4}
	0.4	-1.2×10^{-4}	−0.0018	−0.0026	−0.0027	−0.0028
	0.5	-3.0×10^{-4}	−0.0044	−0.0064	−0.0066	−0.0067
	0.6	-6.3×10^{-4}	−0.0094	−0.0134	−0.0138	−0.0141
	0.7	−0.0012	−0.0186	−0.0261	−0.0270	−0.0275
	0.8	−0.0020	−0.0359	−0.0499	−0.0517	−0.0527
	0.9	−0.0033	−0.0722	−0.1027	−0.1067	−0.1095
	0.99	−0.0049	−0.1526	−0.3486	−0.3640	−0.3852
	0.999	−0.0051	−0.1665	−0.4881	−0.6124	−0.8240
0.25	0.1	2.0×10^{-5}	2.5×10^{-4}	3.3×10^{-4}	3.4×10^{-4}	3.4×10^{-4}
	0.2	7.6×10^{-5}	9.9×10^{-4}	0.0013	0.0013	0.0013
	0.3	1.5×10^{-4}	0.0020	0.0027	0.0027	0.0028
	0.4	2.2×10^{-4}	0.0031	0.0040	0.0041	0.0041
	0.5	2.3×10^{-4}	0.0036	0.0045	0.0045	0.0046
	0.6	1.4×10^{-4}	0.0026	0.0029	0.0028	0.0028
	0.7	-1.2×10^{-4}	−0.0018	−0.0031	−0.0035	−0.0037
	0.8	-6.6×10^{-4}	−0.0134	−0.0190	−0.0201	−0.0209
	0.9	−0.0016	−0.0431	−0.0627	−0.0658	−0.0681
	0.99	−0.0028	−0.1169	−0.2994	−0.3136	−0.3121
	0.999	−0.0030	−0.1301	−0.4384	−0.5610	−0.7720

doi:10.6342/NTU202502370

Table 4. Resistance coefficients for the translation and rotation of a composite sphere where $\lambda b = 1$ parallel to two planar walls, with different values of $d/(d+c)$, b/d, and a/b.

$d/(d+c)$	b/d	a/b = 0.8			a/b = 0.95		
		F_t	T_r	F_r	F_t	T_r	F_r
0	0.1	1.0472	1.0002	-4.0×10^{-6}	1.0564	1.0003	-9.3×10^{-6}
	0.2	1.0987	1.0013	-6.3×10^{-5}	1.1189	1.0022	-1.4×10^{-4}
	0.3	1.1551	1.0044	-3.1×10^{-4}	1.1885	1.0073	-7.0×10^{-4}
	0.4	1.2170	1.0105	-9.5×10^{-4}	1.2669	1.0176	−0.0022
	0.5	1.2857	1.0209	−0.0023	1.3567	1.0355	−0.0052
	0.6	1.3632	1.0371	−0.0046	1.4627	1.0642	−0.0108
	0.7	1.4523	1.0612	−0.0087	1.5932	1.1095	−0.0208
	0.8	1.5581	1.0966	−0.0152	1.7655	1.1831	−0.0385
	0.9	1.6893	1.1493	−0.0257	2.0243	1.3154	−0.0734
	0.99	1.8435	1.2215	−0.0413	2.4836	1.5924	−0.1525
	0.999	1.8617	1.2307	−0.0434	2.5641	1.6447	−0.1681
0.25	0.1	1.0552	1.0002	1.8×10^{-4}	1.0660	1.0003	2.9×10^{-4}
	0.2	1.1163	1.0013	7.1×10^{-4}	1.1405	1.0022	0.0012
	0.3	1.1841	1.0046	0.0015	1.2248	1.0076	0.0024
	0.4	1.2595	1.0109	0.0025	1.3208	1.0183	0.0037
	0.5	1.3439	1.0217	0.0033	1.4314	1.0368	0.0044
	0.6	1.4394	1.0384	0.0037	1.5616	1.0665	0.0035
	0.7	1.5490	1.0633	0.0030	1.7200	1.1131	-6.4×10^{-4}
	0.8	1.6778	1.0998	0.0006	1.9241	1.1883	−0.0115
	0.9	1.8346	1.1538	−0.0053	2.2186	1.3227	−0.0383
	0.99	2.0144	1.2274	−0.0161	2.7136	1.6019	−0.1093
	0.999	2.0353	1.2367	−0.0177	2.7979	1.6545	−0.1239

doi:10.6342/NTU202502370

3.1. Resistance coefficients for a porous particle

The resistance coefficients, F_t, T_r, and F_r, for the translation and rotation of a porous sphere ($a = 0$) parallel to one or two planar walls are plotted against the parameters λb, b/d, and $d/(d+c)$ over the entire range in Figures 2–4, respectively. Similar to the circumstances of the translation and rotation of a porous sphere normal to one or two planar walls [28,29], for fixed values of the parameters $d/(d+c)$ and λb, Figures 3 and 4 and Tables 1 and 2 show that the normalized hydrodynamic drag force and torque that act on the porous particle that translates and rotates parallel to one or two planar walls (or F_t and T_r, respectively) are monotonic increasing functions of the particle–wall spacing parameter, b/d, from zero to unity (note that F_t and T_r are still finite even if the particle touches the planar walls). For the given values of b/d and λb, the drag force and torque increase with an increase in $d/(d+c)$ from zero (the case of a particle translating and rotating parallel to a single planar wall) to 1/2, as shown in Figures 2 and 4. That is, the approach of a second planar wall will enhance the hydrodynamic force and torque exerted on the particle near the first wall. For a fixed value of $2b/(c+d)$ (ratio of particle diameter to wall distance), F_t and T_r are minimal (the particle experiences minimum drag force and torque) when the particle is halfway between the two walls [$d/(d+c) = 1/2$] and increases monotonically as the particle approaches either wall, as shown by the dashed lines in Figure 4.

doi:10.6342/NTU202502370

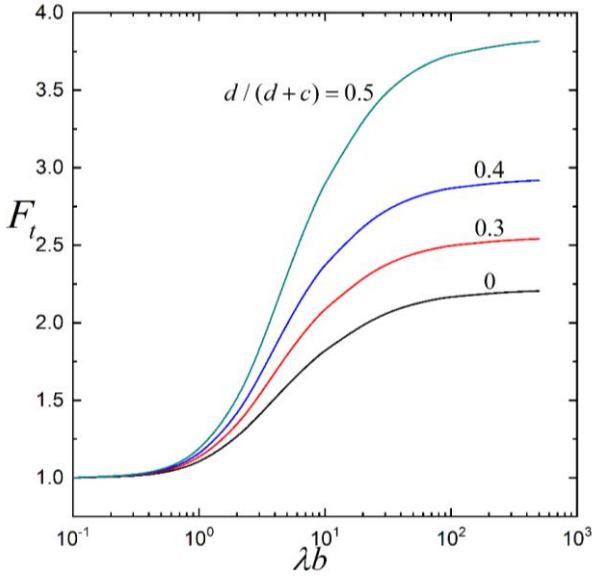

(a)

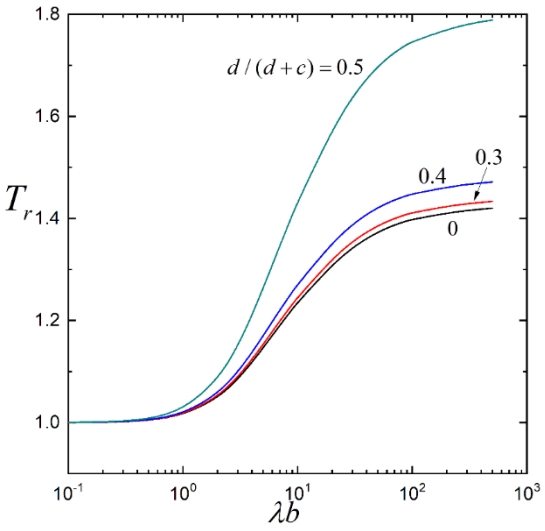

(b)

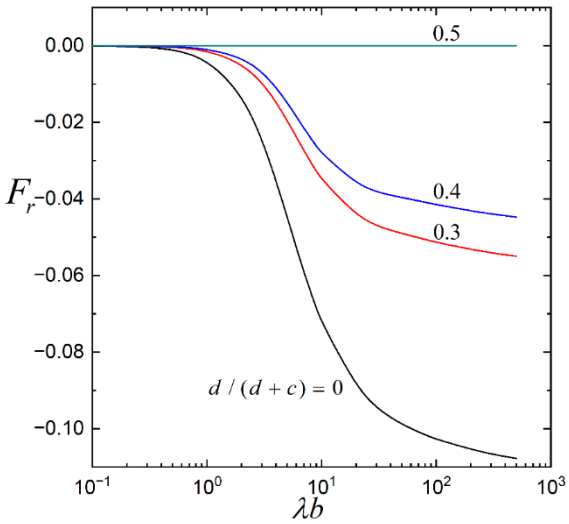

(c)

Figure 2. Resistance coefficients for the motions of a porous sphere ($a=0$) parallel to two planar walls versus the shielding parameter, λb , with $b/d=0.9$ and various values of $d/(d+c)$: (**a**) F_t; (**b**) T_r; (**c**) F_r.

doi:10.6342/NTU202502370

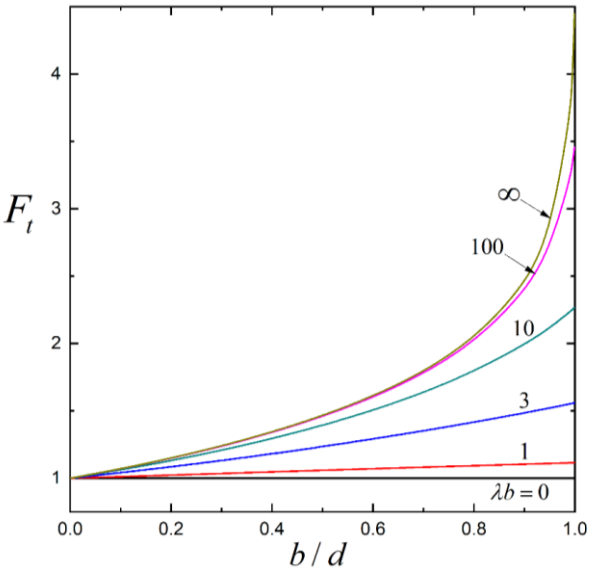

(**a**)

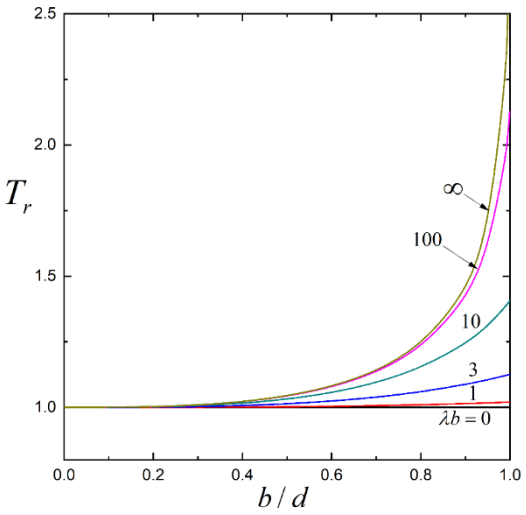

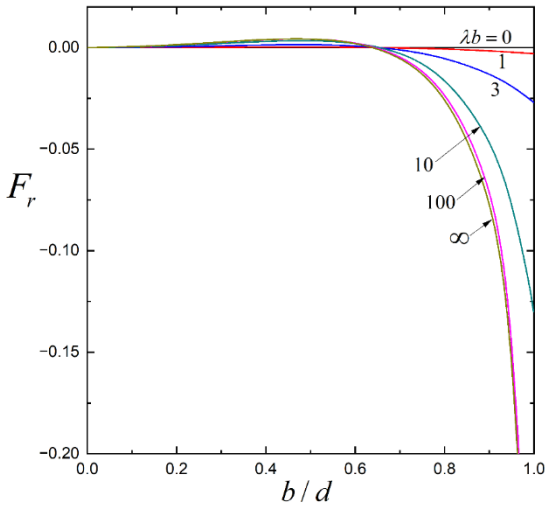

(**b**) (**c**)

Figure 3. Resistance coefficients for the motions of a porous sphere ($a = 0$) parallel to two planar walls versus the spacing parameter, b/d , with $d/(d+c) = 0.25$ and various value of λb : (**a**) F_t ; (**b**) T_r ; (**c**) F_r .

doi:10.6342/NTU202502370

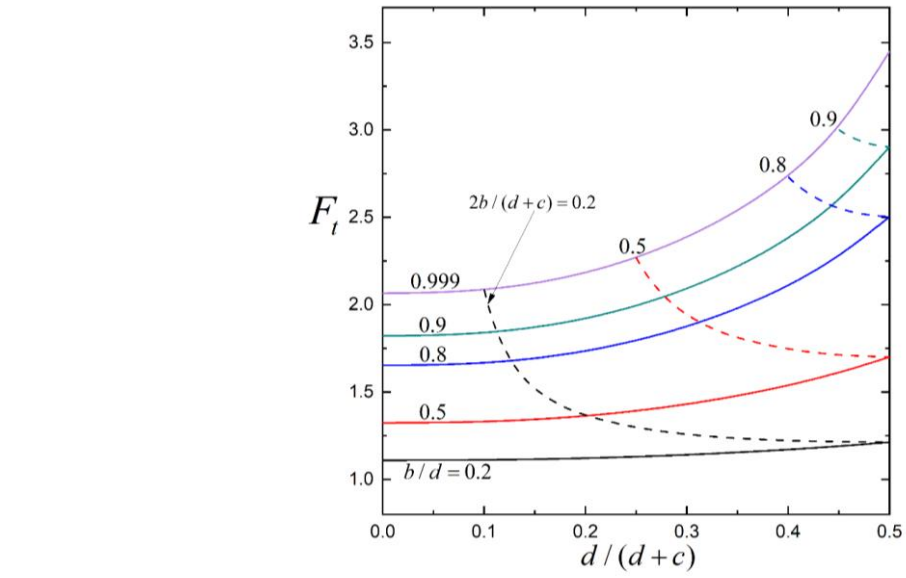

(a)

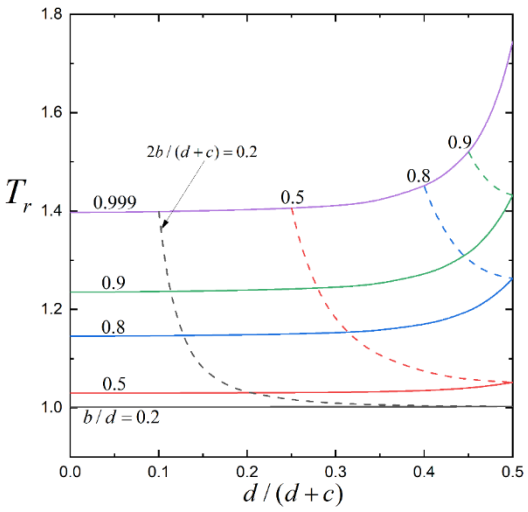

(b)

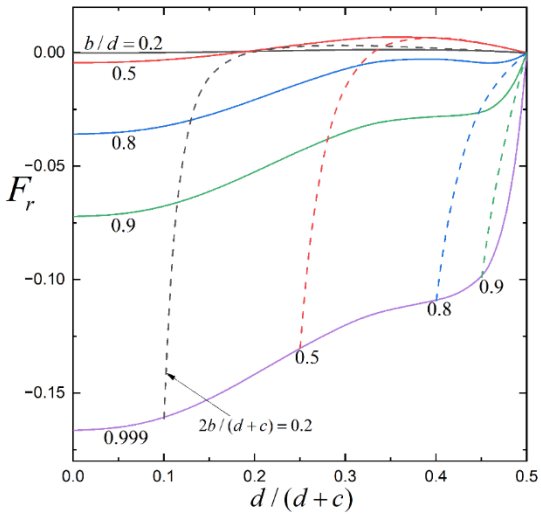

(c)

Figure 4. Resistance coefficients for the motions of a porous sphere ($a=0$) parallel to two planar walls versus the relative particle position parameter, $d/(d+c)$, with $\lambda b=10$ and various values of b/d and $2b/(d+c)$: (**a**) F_t; (**b**) T_r; (**c**) F_r.

doi:10.6342/NTU202502370

As demonstrated in Figures 2 and 3, the force and torque coefficients, F_t and T_r, for the translation and rotation of a porous sphere increase monotonically with an increasing ratio of particle radius to permeation length, λb, from unity at $\lambda b = 0$ (with $F_0 = F = 0$ and $T_0 = T = 0$) for given values of b/d and $d/(d+c)$. On the other hand, as revealed in Figures 3 and 4 and Table 3, the coupling coefficient, F_r, is not necessarily a monotonic function of the parameters b/d, $d/(d+c)$, and λb [there may be extrema at moderate values of b/d, $d/(d+c)$, and λb], fixing the other parameters. When λb is smaller than unity, the variations of all the resistance coefficients, F_t, T_r, and F_r, with b/d and $d/(d+c)$ are weak. In general, these resistance coefficients for a porous sphere with $\lambda b \geq 100$ is sufficiently close to those of a hard sphere (with $\lambda b \to \infty$). A comparison of Figures 2–4 and Tables 1 and 2 shows that the boundary effects of the planar walls on the translation of the particle are much more conspicuous than those on the rotation.

doi:10.6342/NTU202502370

3.2 Resistance coefficients for a composite particle

The force, torque, and coupling coefficients, F_t, T_r, and F_r, for the translation and rotation of a general composite spherical particle parallel to one or two planar walls are plotted in Figures 5–7 for various values of the core-to-particle radius ratio, a/b, particle–wall spacing parameter, b/d, relative particle position parameter, $d/(d+c)$, and ratio of particle radius to porous layer permeation length, λb. Similarly, F_t and T_r increase monotonically with increases in b/d, λb, and $d/(d+c)$, fixing the other parameters. For a fixed value of $2b/(c+d)$, F_t and T_r are minimal at $d/(d+c)=1/2$ and increase monotonically with a decrease in $d/(d+c)$. The coupling coefficient, F_r, is not necessarily a monotonic function of b/d, λb, and $d/(d+c)$, keeping other parameters unchanged. The boundary effects of the planar walls on the translation of the composite particle are much more noticeable than the effects on the rotation.

doi:10.6342/NTU202502370

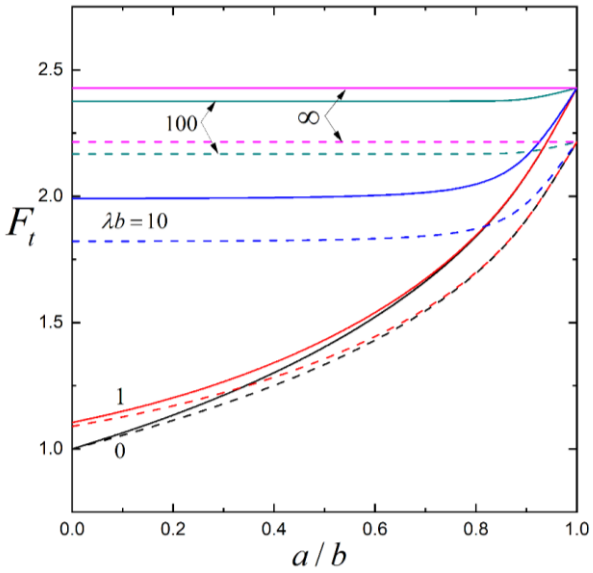

(a)

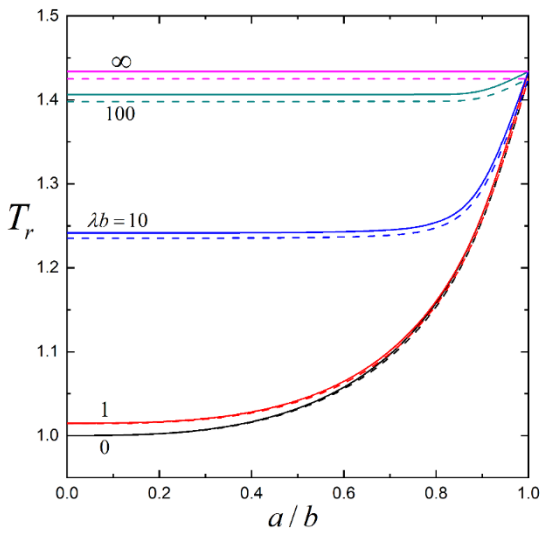

(b)

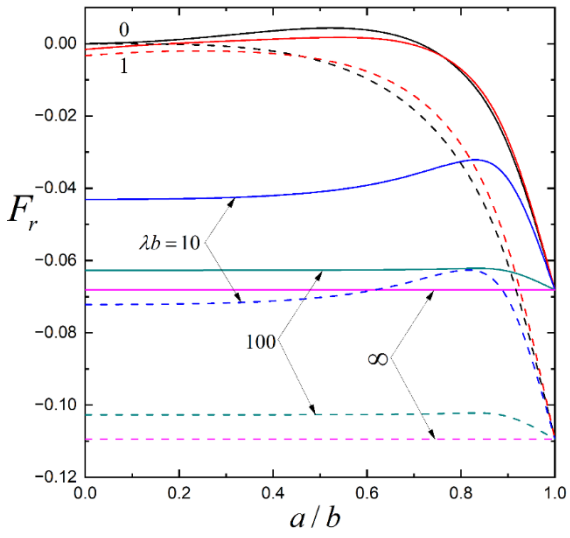

(c)

Figure 5. Resistance coefficients for the motions of a composite sphere parallel to two planar walls versus the core-to-particle radius ratio, a/b, with $b/d = 0.9$ and various values of λb: (**a**) F_t; (**b**) T_r; (**c**) F_r. The solid and dashed curves denote cases of $d/(d+c) = 0.25$ and $d/(d+c) = 0$, respectively.

doi:10.6342/NTU202502370

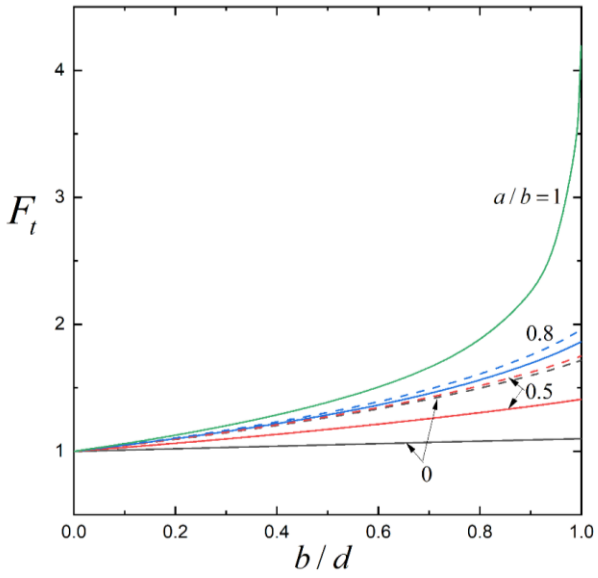

(a)

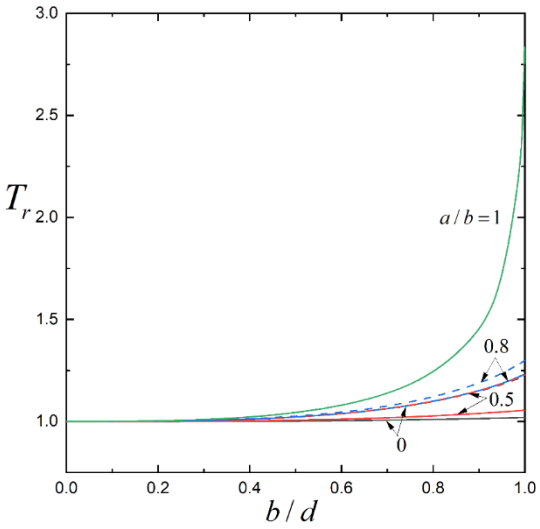

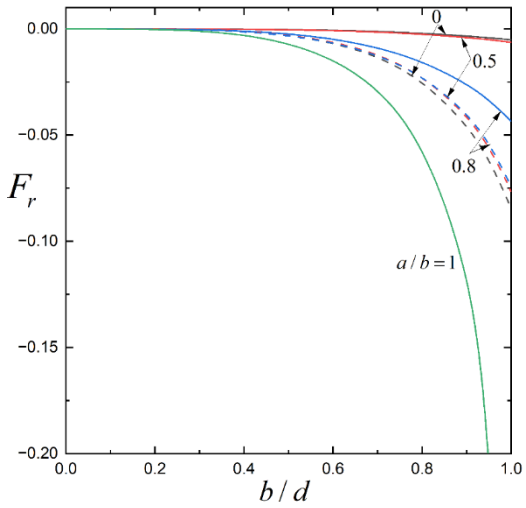

(b) **(c)**

Figure 6. Resistance coefficients for the motions of a composite sphere parallel to two planar walls versus the spacing parameter, b/d, with $d/(d+c)=0$ and various values of a/b: **(a)** F_t; **(b)** T_r; **(c)** F_r. The solid and dashed curves denote cases of $\lambda b=1$ and $\lambda b=5$, respectively.

doi:10.6342/NTU202502370

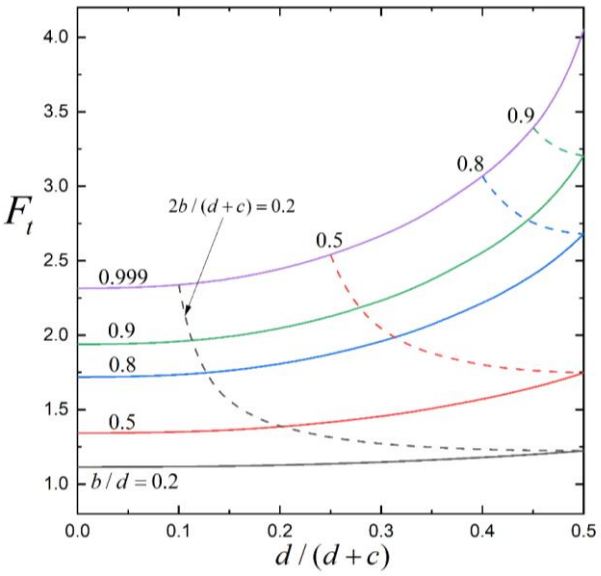

(a)

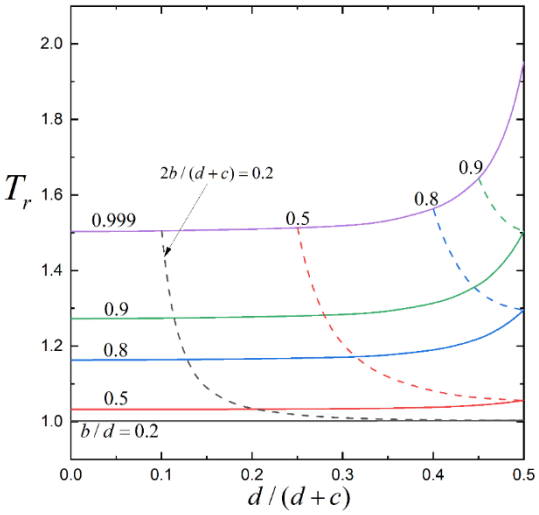

(b)

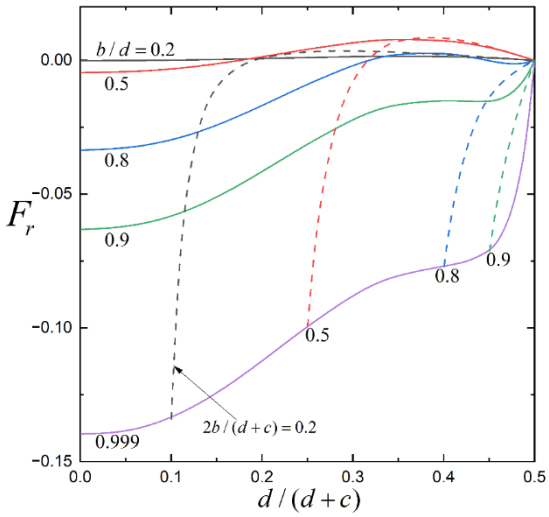

(c)

Figure 7. Resistance coefficients for the motions of a composite sphere parallel to two planar walls versus the relative position parameter, $d/(d+c)$, with $\lambda b=10$, $a/b=0.9$, and various values of b/d and $2b/(d+c)$: (**a**) F_t; (**b**) T_r; (**c**) F_r.

doi:10.6342/NTU202502370

For specified values of b/d, λb, and $d/(d+c)$, Table 4 and Figures 5–7 demonstrate that the force and torque coefficients, F_t and T_r, of a composite sphere that translates and rotates parallel to one or two planar walls monotonically increase with an increase in the radius ratio, a/b (a decrease in the relative thickness of the porous layer), where the limits $a/b=1$ and $a/b=0$ denote a hard sphere and an entirely porous sphere, respectively. All hydrodynamic force and torque results for a general composite sphere fall between the lower and upper limits of $a/b=0$ and $a/b=1$, respectively. On the other hand, the coupling coefficient, F_r, is not necessarily a monotonic function of a/b for fixed values of b/d, λb, and $d/(d+c)$. When the porous layer of the composite particle has small to moderate permeability (say, $\lambda b>10$), as shown in Figure 5, the values of all the resistance coefficients, F_t, T_r, and F_r, of the composite particle with $a/b<0.8$ can be well approximated using the values of a fully porous particle with the same b/d, λb, and $d/(d+c)$. Namely, the hard core of the composite sphere can hardly feel the relative fluid motion and only exerts negligible hydrodynamic resistance. However, this approximation does not apply to highly permeable porous layers.

Since the governing equations of the general problem for a composite sphere translating and rotating in arbitrary directions near one or two planar walls are linear, its solution can be determined by the superposition of the solutions to its two subproblems: motions parallel to the planar walls, which are examined in this thesis, and motions

doi:10.6342/NTU202502370

normal to the planar walls. The collocation solutions for the translation and rotation of a composite sphere normal to the planar walls were previously obtained [28,29], and it was found that the wall-corrected normalized drag force and torque acting on the particle also increase with increases in b/d, λb, $d/(d+c)$, and a/b. Interestingly, comparisons between those results and our solutions indicate that the planar walls exert much more force but less torque on the particle when its translational and rotational motions occur normal to them than when its motions occur parallel to them. Therefore, the directions of translation and rotation of a composite sphere near one or two planar walls are different from those of the imposed force and torque, respectively, except when the directions are parallel or normal to the walls. The concepts discussed above are summarized in the schematic diagram shown in Figure 8.

doi:10.6342/NTU202502370

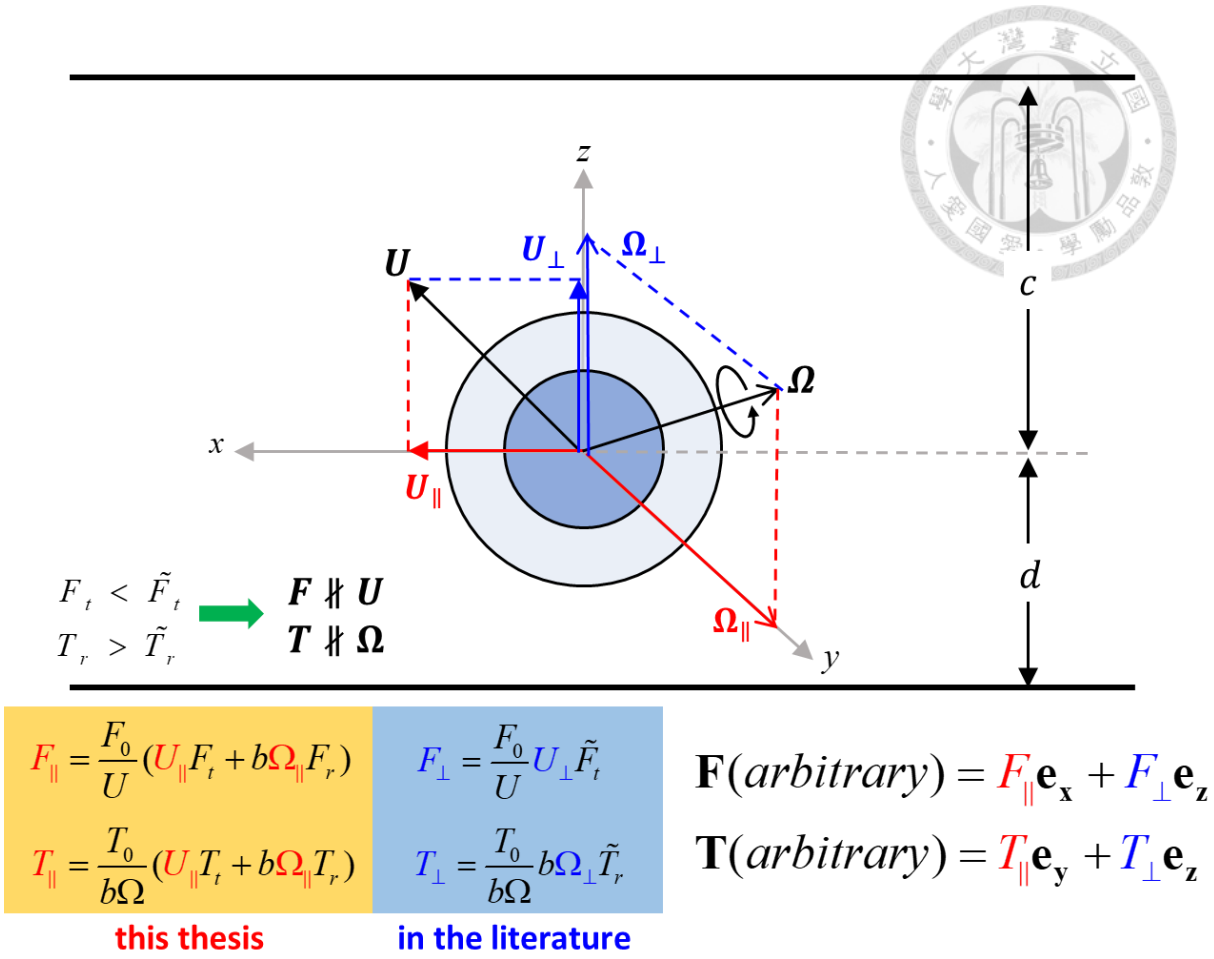

$$F_{\parallel}=\frac{F_0}{U}(U_{\parallel}F_t+b\Omega_{\parallel}F_r) \qquad F_{\perp}=\frac{F_0}{U}U_{\perp}\tilde{F}_t$$

$$T_{\parallel}=\frac{T_0}{b\Omega}(U_{\parallel}T_t+b\Omega_{\parallel}T_r) \qquad T_{\perp}=\frac{T_0}{b\Omega}b\Omega_{\perp}\tilde{T}_r$$

this thesis | in the literature

$$\mathbf{F}(arbitrary)=F_{\parallel}\mathbf{e}_x+F_{\perp}\mathbf{e}_z$$

$$\mathbf{T}(arbitrary)=T_{\parallel}\mathbf{e}_y+T_{\perp}\mathbf{e}_z$$

Figure 8. Summary of the key concepts for the translation and rotation a composite sphere in arbitrary directions and at an arbitrary position between two planar walls.

In Tables 1–4 and Figures 2–7, we present detailed results pertaining to the resistance problem, which involves evaluating the hydrodynamic force, $\mathbf{F}$, and torque, $\mathbf{T}$, experienced by a composite sphere undergoing prescribed translational and angular velocities, $\mathbf{U}$ and $\mathbf{\Omega}$, respectively, parallel to one or two planar walls under steady conditions. In contrast, the mobility problem entails determining the resulting particle velocities, $\mathbf{U}$ and $\mathbf{\Omega}$, when known external force, $\mathbf{F}$, and torque, $\mathbf{T}$, are applied to the composite sphere. For the specific case of the slow translation and rotation of the

doi:10.6342/NTU202502370

composite sphere considered in this thesis, the analytical formulations provided in Equation (19) are equally applicable to the corresponding mobility problem. In particular, for configurations involving free rotational motion parallel to one or two planar walls driven solely by an external force, $\mathbf{F}$, the resulting translational and angular velocities of the composite sphere can be directly obtained via Equation (19), with the following result:

$$U = \frac{F}{F_0 / U}(F_{\mathrm{t}} - F_{\mathrm{r}} \frac{T_{\mathrm{t}}}{T_{\mathrm{r}}})^{-1}, \tag{21a}$$

$$\Omega = -\frac{U}{b} \frac{T_{\mathrm{t}}}{T_{\mathrm{r}}}, \tag{21b}$$

where the resistance coefficients are presented in the aforementioned tables and figures, and the term F_0 / U that appears on the right-hand side of Equation (21a) can be evaluated using Equation (1).

doi:10.6342/NTU202502370

Chapter 4

Conclusions

The low-Reynolds number-coupled translational and rotational motions of a composite spherical particle (hard core with porous surface layer) in a viscous fluid parallel to one or two planar walls are investigated semi-analytically using a method of boundary collocation. When the core-to-particle radius ratio, a/b, ratio of particle radius to porous layer permeation length, λb, particle–wall spacing parameter, b/d, and relative particle position parameter, $d/(d+c)$, take arbitrary values, convergent numerical results of the hydrodynamic force and torque acting on the particle are obtained. The normalized drag force and torque increase monotonically with increases in a/b, b/d, λb, and $d/(d+c)$, keeping other parameters unchanged. For a fixed value of the ratio of particle diameter to wall-to-wall distance, $2b/(c+d)$, these force and torque are minimal at $d/(d+c)=1/2$ (as the particle is midway between the two walls) and increase steadily with a decrease in $d/(d+c)$ (shorter distance to either wall). The coupling between the translation and rotation of the composite sphere parallel to the walls exhibits complex behavior that does not vary monotonically with changes in system parameters. The influence of the walls on translational motion is significantly stronger

doi:10.6342/NTU202502370

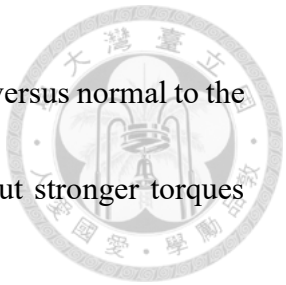

than on rotational motion. When comparing particle motions parallel versus normal to the walls, the planar boundaries impose weaker hydrodynamic forces but stronger torques during parallel motions.

doi:10.6342/NTU202502370

List of Symbols

a	the radius of hard core, m
A_n, B_n, C_n	unknown constants in Eq. (13) and Eq. (14), $m^{n+1} \cdot s^{-1}$, $m^{n+3} \cdot s^{-1}$, $m^{n+2} \cdot s^{-1}$
A_n', B_n', C_n'	functions of position defined by Eq. (2.6) of Ganatos et al. [13], m^{-n}, m^{-n-2}, m^{-n-1}
A_n'', B_n'', C_n''	functions of position defined by Eq. (2.6) of Ganatos et al. [13], m^{-n}, m^{-n-2}, m^{-n-1}
A_n''', B_n''', C_n'''	functions of position defined by Eq. (2.6) of Ganatos et al. [13], m^{-n}, m^{-n-2}, m^{-n-1}
$A_n'''', B_n'''', C_n''''$	functions of position defined by Eqs. (A10)–(A12) in Appendix A, m^{-n-1}, m^{-n-3}, m^{-n-2}
A_n^*, B_n^*, C_n^*	functions of position defined by Eq. (11) of Chen and Keh [14], m^{-n}, m^{-n-2}, m^{-n-1}
$A_n^{**}, B_n^{**}, C_n^{**}$	functions of position defined by Eq. (11) of Chen and Keh [14], m^{-n}, m^{-n-2}, m^{-n-1}
$A_n^{***}, B_n^{***}, C_n^{***}$	functions of position defined by Eq. (11) of Chen and Keh [14], m^{-n}, m^{-n-2}, m^{-n-1}

doi:10.6342/NTU202502370

b	the radius of the composite spherical particle, m
$B_{n,m,j,l}(z)$	a function defined by Eq. (C5) of Ganatos et al. [13].
$\hat{C}_{1n},\hat{C}_{2n},\hat{C}_{3n},\hat{C}_{4n}$	unknown constants in Eq. (16) and Eq. (17), $m^{-n+2}\cdot s^{-1}$, $m^{n+3}\cdot s^{-1}$, $m^{5/2}\cdot s^{-1}$, $m^{5/2}\cdot s^{-1}$
c,d	the distances of the planar walls from the particle center, m
$\hat{D}_{1n},\hat{D}_{2n}$	unknown constants in Eq. (16), $m^{3/2}\cdot s^{-1}$, $m^{3/2}\cdot s^{-1}$
$\mathbf{e}_x,\mathbf{e}_y,\mathbf{e}_z$	the principal unit vectors in the Cartesian coordinates, -, -, -
$\mathbf{e}_r,\mathbf{e}_\theta,\mathbf{e}_\phi$	the principal unit vectors in the spherical coordinates, -, -, -
$\mathbf{F},F$	the force exerted by the fluid on the composite particle in the presence of planar walls, N
$\mathbf{F_0},F_0$	the force exerted by the fluid on the composite particle in an unbounded fluid, N
F_t	the force coefficient defined by Eq. (19a), -
F_r,T_t	the coupling coefficients defined by Eq. (19), -
G_1,G_2	constants defined by Eq. (3), -
$\mathbf{I}$	the unit tensor, -
I_n	the modified Bessel function of the first kind of order n, -
J_1	the Bessel function of the first kind of order one, -
K_n	the modified Bessel function of the second kind of order n, -

doi:10.6342/NTU202502370

p	the fluid pressure outside the composite sphere, $\mathrm{N}\cdot\mathrm{m}^{-2}$
$\hat{p}$	the fluid pressure within the porous surface layer, $\mathrm{N}\cdot\mathrm{m}^{-2}$
P_n^1	the associated Legendre function of the first kind of order n and degree 1, -
r,θ,ϕ	spherical coordinates, m, -, -
$\mathbf{r}$	the position vector ($= r\mathbf{e}_r$), m
$\mathbf{T},T$	the torque exerted by the fluid on the composite particle in the presence of planar walls, $\mathrm{N}\cdot\mathrm{m}$
$\mathbf{T_0},T_0$	the torque exerted by the fluid on the composite particle in an unbounded fluid, $\mathrm{N}\cdot\mathrm{m}$
T_r	the torque coefficient defined by Eq. (19b), -
$\mathbf{U},U$	the translational velocity of the composite particle, $m\cdot s^{-1}$
$\mathbf{v}$	the fluid velocity distribution outside the composite sphere, $\mathrm{m}\cdot\mathrm{s}^{-1}$
$\hat{\mathbf{v}}$	the fluid velocity distribution within the porous surface layer, $\mathrm{m}\cdot\mathrm{s}^{-1}$
v_x,v_y,v_z	x, y and z components of the external fluid velocity, $\mathrm{m}\cdot\mathrm{s}^{-1}$
v_r,v_θ,v_ϕ	r, θ and ϕ components of the external fluid velocity, $\mathrm{m}\cdot\mathrm{s}^{-1}$
$\hat{v}_r,\hat{v}_\theta,\hat{v}_\phi$	r, θ and ϕ components of the internal fluid velocity, $\mathrm{m}\cdot\mathrm{s}^{-1}$
V	a constant defined by Eq. (4), -

doi:10.6342/NTU202502370

W	a constant defined by Eq. (4), -
x, y, z	Cartesian coordinates, m, m, m

Greek letters

μ	$=\cos\theta$, -
η	the viscosity of the fluid, $\mathrm{kg\cdot m^{-1}\cdot s^{-1}}$
λ^{-1}	the penetration length (square root of permeability) of fluid flow within the porous surface layer of the composite particle, m
ρ, ϕ, z	circular cylindrical coordinates, m, -, m
$\boldsymbol{\tau}$	the viscous stress tensor for the external flow, $\mathrm{N\cdot m^{-2}}$
$\hat{\boldsymbol{\tau}}$	the viscous stress tensor for the internal flow, $\mathrm{N\cdot m^{-2}}$
$\boldsymbol{\Omega}, \Omega$	the angular velocity of the composite particle, $\mathrm{s^{-1}}$
$\alpha_n', \beta_n', \gamma_n'$	functions of position defined by Eq. (C1) of Ganatos et al. [13], m^{-n}, m^{-n-2}, m^{-n-1}
$\alpha_n'', \beta_n'', \gamma_n''$	functions of position defined by Eq. (C1) of Ganatos et al. [13], m^{-n}, m^{-n-2}, m^{-n-1}
$\alpha_n''', \beta_n''', \gamma_n'''$	functions of position defined by Eq. (C1) of Ganatos et al. [13], m^{-n}, m^{-n-2}, m^{-n-1}

doi:10.6342/NTU202502370

References

1. Stokes, G.G. On the theories of the internal friction of fluids in motion and of the equilibrium and motion of elastic solids. *Trans. Camb. Phil. Soc.* **1845**, *8*, 287–319.
2. Stokes, G.G. On the effect of the internal friction of fluids on the motion of pendulums. *Trans. Cambridge Phil. Soc.* **1851**, *9*, 8–106.
3. Masliyah, J.H.; Neale, G.; Malysa, K.; van de Ven, T.G.M. Creeping flow over a composite sphere: Solid core with porous shell. *Chem. Eng. Sci.* **1987**, *42*, 245–253.
4. Keh, H.J.; Chou, J. Creeping motion of a composite sphere in a concentric spherical cavity. *Chem. Eng. Sci.* **2004**, *59*, 407–415.
5. Wunderlich, R.W. The effects of surface structure on the electrophoretic mobilities of large particles. *J. Colloid Interface Sci.* **1982**, *88*, 385–397.
6. Anderson, J.L.; Solomentsev, Y. Hydrodynamic effects of surface layer on colloidal particles. *Chem. Eng. Comm.* **1996**, *148–150*, 291–314.
7. Napper, D.H. *Polymeric Stabilization of Colloidal Dispersions*; Academic Press: London, UK, 1983.
8. Neale, G.; Epstein, N.; Nader, W. Creeping flow relative to permeable spheres. *Chem. Eng. Sci.* **1973**, *28*, 1865–1874.

doi:10.6342/NTU202502370

9. Happel, J.; Brenner, H. *Low Reynolds Number Hydrodynamics*; Nijhoff: Dordrecht, The Netherlands, 1983.

10. Anderson, J.L. Colloid transport by interfacial forces. *Ann. Rev. Fluid Mech.* **1989**, *21*, 61–99.

11. Romanò, F.; des Boscs, P.-E.; Kuhlmann, H.C. Forces and torques on a sphere moving near a dihedral corner in creeping flow. *Eur. J. Mech. B Fluids* **2020**, *84*, 110–121.

12. Goldman, A.J.; Cox, R.G.; Brenner, H. Slow viscous motion of a sphere parallel to a plane wall-I. Motion through a quiescent fluid. *Chem. Eng. Sci.* **1967**, *22*, 637–651.

13. Ganatos, P.; Pfeffer, R.; Weinbaum, S. A strong interaction theory for the creeping motion of a sphere between plane parallel boundaries. Part 2. Parallel motion. *J. Fluid Mech.* **1980**, *99*, 755–783.

14. Chen, P.Y.; Keh, H.J. Slow motion of a slip spherical particle parallel to one or two plane walls. *J. Chin. Inst. Chem. Engrs.* **2003**, *34*, 123–133.

15. Sherief, H.H.; Faltas, M.S.; Ashmawy, E.A.; Nashwan, M.G. Slow motion of a slip spherical particle along the axis of a circular cylindrical pore in a micropolar fluid. *J. Mol. Liq.* **2014**, *200*, 273–282.

16. Papavassiliou, D.; Alexander, G.P. Exact solutions for hydrodynamic interactions of two squirming spheres. *J. Fluid Mech.* **2017**, *813*, 618–646.

doi:10.6342/NTU202502370

17. Chou, C.Y.; Keh, H.J. Slow rotation of a spherical particle in an eccentric spherical cavity with slip surfaces. *Eur. J. Mech. B Fluids* **2021**, *86*, 150–156.
18. Lee, M.C.; Keh, H.J. Slow axisymmetric rotation of a sphere in a circular tube with slip surfaces. *Fluid Dyn. Res.* **2021**, *53*, 065502.
19. Nashwan, M.G.; Ragab, K.E.; Faltas, M.S. Axisymmetric slow motion of a non-deformable spherical droplet or slip particle toward an orifice in a plane wall. *Phys. Fluids* **2022**, *34*, 083106.
20. Liao, J.C.; Keh, H.J. Slow rotation of a sphere about its diameter normal to two planes with slip surfaces. *Fluid Dyn. Res.* **2022**, *54*, 035502.
21. Madasu, K.P. Boundary effects of slow flow past a fluid coated sphere. *Phys. Fluids* **2025**, *37*, 031908.
22. Srinivasacharya, D.; Krishna Prasad, M. Steady rotation of a composite sphere in a concentric spherical cavity. *Acta Mech. Sin.* **2012**, *28*, 653–658.
23. Prakash, J.; Raja Sekhar, G.P. Slow motion of a porous spherical particle with a rigid core in a spherical fluid cavity. *Meccanica* **2017**, *52*, 91–105.
24. Chou, C.Y.; Keh, H.J. Low-Reynolds-number rotation of a soft particle inside an eccentric cavity. *Eur. J. Mech. B Fluids* **2022**, *91*, 194–201.
25. Chen, Y.C.; Keh, H.J. Slow translation of a composite sphere in an eccentric spherical cavity. *Fluids* **2024**, *9*, 154.

doi:10.6342/NTU202502370

26. Chen, Y.C.; Keh, H.J. Slow translation and rotation of a composite sphere within a nonconcentric spherical cavity normal to their common diameter. *Fluid Dyn. Res.* **2025**, *54*, 035502.

27. Jhuang, L.J.; Keh, H.J. Slow axisymmetric rotation of a soft sphere in a circular cylinder. *Eur. J. Mech. B Fluids* **2022**, *95*, 205–211.

28. Chen, S.B.; Ye, X. Boundary effect on slow motion of a composite sphere perpendicular to two parallel impermeable plates. *Chem. Eng. Sci.* **2000**, *55*, 2441–2453.

29. Chang, C.L.; Keh, H.J. Slow rotation of a soft colloidal sphere normal to two plane walls. *Colloids Interfaces* **2023**, *7*, 18.

30. Koplik, J.; Levine, H.; Zee, A. Viscosity renormalization in the Brinkman equation. *Phys. Fluids* **1983**, *26*, 2864–2870.

doi:10.6342/NTU202502370

Appendix A

A.1. Some lengthy equations in Chapter 2

By substituting Equations (12)–(17) into Equations (7) and (8), we obtain

$$\sum_{n=1}^{\infty} n(n+1)P_n^1(\mu)\{\hat{C}_{1n}a^{n-1}+\hat{C}_{2n}a^{-n-2}+a^{-3/2}[\hat{C}_{3n}I_{n+1/2}(\lambda a)+\hat{C}_{4n}K_{n+1/2}(\lambda a)]\}=0, \tag{A1}$$

$$\begin{aligned}\sum_{n=1}^{\infty}\{&[-\hat{C}_{1n}(n+1)a^{n-1}+n\hat{C}_{2n}a^{-n-2}+\hat{C}_{3n}\{na^{-3/2}I_{n+1/2}(\lambda a)-\lambda a^{-1/2}I_{n-1/2}(\lambda a)\}\\&+\hat{C}_{4n}\{na^{-3/2}K_{n+1/2}(\lambda a)+\lambda a^{-1/2}K_{n-1/2}(\lambda a)\}](1-\mu^2)^{1/2}\frac{\mathrm{d}P_n^1(\mu)}{\mathrm{d}\mu}\\&+a^{-1/2}[\hat{D}_{1n}I_{n+1/2}(\lambda a)+\hat{D}_{2n}K_{n+1/2}(\lambda a)](1-\mu^2)^{-1/2}P_n^1(\mu)\}=0,\end{aligned} \tag{A2}$$

$$\begin{aligned}\sum_{n=1}^{\infty}\{&[-\hat{C}_{1n}(n+1)a^{n-1}+n\hat{C}_{2n}a^{-n-2}+\hat{C}_{3n}\{na^{-3/2}I_{n+1/2}(\lambda a)-\lambda a^{-1/2}I_{n-1/2}(\lambda a)\}\\&+\hat{C}_{4n}\{na^{-3/2}K_{n+1/2}(\lambda a)+\lambda a^{-1/2}K_{n-1/2}(\lambda a)\}](1-\mu^2)^{-1/2}P_n^1(\mu)\\&+a^{-1/2}[\hat{D}_{1n}I_{n+1/2}(\lambda a)+\hat{D}_{2n}K_{n+1/2}(\lambda a)](1-\mu^2)^{1/2}\frac{\mathrm{d}P_n^1(\mu)}{\mathrm{d}\mu}\}=0,\end{aligned} \tag{A3}$$

$$\sum_{n=1}^{\infty}\{[A_nA_n''''+B_nB_n''''+C_nC_n'''']_{r=b}+\lambda^2[(n+1)\hat{C}_{1n}b^n-n\hat{C}_{2n}b^{-n-1}]P_n^1(\mu)\cos\phi\}=0, \tag{A4}$$

$$\begin{aligned}\sum_{n=1}^{\infty}\{&[A_nA_n^*+B_nB_n^*+C_nC_n^*]_{r=b}\sec\phi-n(n+1)[\hat{C}_{1n}b^{n-1}+\hat{C}_{2n}b^{-n-2}\\&+b^{-3/2}\{\hat{C}_{3n}I_{n+1/2}(\lambda b)+\hat{C}_{4n}K_{n+1/2}(\lambda b)\}]P_n^1(\mu)\}-U(1-\mu^2)^{1/2}=0,\end{aligned} \tag{A5}$$

$$\begin{aligned}\sum_{n=1}^{\infty}\{&[A_nA_n^{**}+B_nB_n^{**}+C_nC_n^{**}]_{r=b}\sec\phi+[\hat{C}_{1n}(n+1)b^{n-1}-n\hat{C}_{2n}b^{-n-2}+\hat{C}_{3n}\{\lambda b^{-1/2}I_{n-1/2}(\lambda b)\\&-nb^{-3/2}I_{n+1/2}(\lambda b)\}-\hat{C}_{4n}\{\lambda b^{-1/2}K_{n-1/2}(\lambda b)+nb^{-3/2}K_{n+1/2}(\lambda b)\}](1-\mu^2)^{1/2}\frac{\mathrm{d}P_n^1(\mu)}{\mathrm{d}\mu}\\&-b^{-1/2}[\hat{D}_{1n}I_{n+1/2}(\lambda b)+\hat{D}_{2n}K_{n+1/2}(\lambda b)](1-\mu^2)^{-1/2}P_n^1(\mu)\}-U\mu-\Omega b=0,\end{aligned} \tag{A6}$$

doi:10.6342/NTU202502370

$$\sum_{n=1}^{\infty}\{[A_nA_n^{***}+B_nB_n^{***}+C_nC_n^{***}]_{r=b}\csc\phi+[\hat{C}_{1n}(n+1)b^{n-1}-n\hat{C}_{2n}b^{-n-2}+\hat{C}_{3n}\{\lambda b^{-1/2}I_{n-1/2}(\lambda b)$$
$$-nb^{-3/2}I_{n+1/2}(\lambda b)\}-\hat{C}_{4n}\{\lambda b^{-1/2}K_{n-1/2}(\lambda b)+nb^{-3/2}K_{n+1/2}(\lambda b)\}](1-\mu^2)^{-1/2}P_n^1(\mu) \quad \text{(A7)}$$
$$-b^{-1/2}[\hat{D}_{1n}I_{n+1/2}(\lambda b)+\hat{D}_{2n}K_{n+1/2}(\lambda b)](1-\mu^2)^{1/2}\frac{\mathrm{d}P_n^1(\mu)}{\mathrm{d}\mu}\}+U+\Omega b\mu=0,$$

$$\sum_{n=1}^{\infty}\{(\frac{\partial}{\partial r}[A_nA_n^{**}+B_nB_n^{**}+C_nC_n^{**}])_{r=b}\sec\phi+[(n+1)(n-1)b^{n-2}\hat{C}_{1n}+n(n+2)b^{-n-3}\hat{C}_{2n}$$
$$-b^{-5/2}([(1-n^2-\lambda^2b^2)I_{n+1/2}(\lambda b)+\lambda bI_{n+3/2}(\lambda b)]\hat{C}_{3n}+[(1-n^2-\lambda^2b^2)K_{n+1/2}(\lambda b)$$
$$-\lambda bK_{n+3/2}(\lambda b)]\hat{C}_{4n})](1-\mu^2)^{1/2}\frac{\mathrm{d}P_n^1(\mu)}{\mathrm{d}\mu}-b^{-3/2}([nI_{n+1/2}(\lambda b)+\lambda bI_{n+3/2}(\lambda b)]\hat{D}_{1n} \quad \text{(A8)}$$
$$+[nK_{n+1/2}(\lambda b)-\lambda bK_{n+3/2}(\lambda b)]\hat{D}_{2n})(1-\mu^2)^{-1/2}P_n^1(\mu)\}-\Omega=0,$$

$$\sum_{n=1}^{\infty}\{(\frac{\partial}{\partial r}[A_nA_n^{***}+B_nB_n^{***}+C_nC_n^{***}])_{r=b}\csc\phi+[(n+1)(n-1)b^{n-2}\hat{C}_{1n}+n(n+2)b^{-n-3}\hat{C}_{2n}$$
$$-b^{-5/2}([(1-n^2-\lambda^2b^2)I_{n+1/2}(\lambda b)+\lambda bI_{n+3/2}(\lambda b)]\hat{C}_{3n}+[(1-n^2-\lambda^2b^2)K_{n+1/2}(\lambda b)$$
$$-\lambda bK_{n+3/2}(\lambda b)]\hat{C}_{4n})](1-\mu^2)^{-1/2}P_n^1(\mu)-b^{-3/2}([nI_{n+1/2}(\lambda b)+\lambda bI_{n+3/2}(\lambda b)]\hat{D}_{1n} \quad \text{(A9)}$$
$$+[nK_{n+1/2}(\lambda b)-\lambda bK_{n+3/2}(\lambda b)]\hat{D}_{2n})(1-\mu^2)^{1/2}\frac{\mathrm{d}P_n^1(\mu)}{\mathrm{d}\mu}\}+\Omega\mu=0,$$

where the starred A_n, B_n, and C_n are functions of position defined by Equation (11) of Chen and Keh [14].

The tetra-primed A_n, B_n, and C_n in Equation (14) are functions of position that are defined by

$$A_n''''(r,\mu,\phi)=2n(2n-1)r^{-n-1}P_n^1(\mu)\cos\phi-\cos\phi\int_0^{\infty}\frac{J_1(\kappa\rho)}{\kappa(\tau^2-\sinh^2\tau)}[2\kappa X_1(\sigma,\eta)Y_{n1}(-d) \quad \text{(A10)}$$
$$-2\kappa X_1(\eta,\sigma)Y_{n1}(c)+X_2(\sigma,\eta)Y_{n2}(-d)-X_2(\eta,\sigma)Y_{n2}(c)]\mathrm{d}\kappa,$$

doi:10.6342/NTU202502370

$$B_n''''(r,\mu,\phi) = -\cos\phi \int_0^\infty \frac{J_1(\kappa\rho)}{\kappa(\tau^2 - \sinh^2\tau)} [2\kappa X_1(\sigma,\eta) n B_{n+1,1,1,2}(-d) - 2\kappa X_1(\eta,\sigma) n B_{n+1,1,1,2}(c) \\ -\kappa^2 X_2(\sigma,\eta) Y_{n4}(-d) + \kappa^2 X_2(\eta,\sigma) Y_{n4}(c)] \mathrm{d}\kappa , \tag{A11}$$

$$C_n''''(r,\mu,\phi) = -\cos\phi \int_0^\infty \frac{J_1(\kappa\rho)}{\kappa(\tau^2 - \sinh^2\tau)} [2\kappa X_1(\sigma,\eta) B_{n,1,1,2}(-d) - 2\kappa X_1(\eta,\sigma) B_{n,1,1,2}(c) \\ -\kappa^2 X_2(\sigma,\eta) Y_{n3}(-d) + \kappa^2 X_2(\eta,\sigma) Y_{n3}(c)] \mathrm{d}\kappa , \tag{A12}$$

where $\sigma = \kappa(z+d)$, $\eta = \kappa(z-c)$, $\tau = \kappa(c+d)$,

$$X_1(\delta,\nu) = \tau\cosh\delta + \cosh\nu\sinh\tau , \tag{A13}$$

$$X_2(\delta,\nu) = \tau\sinh\delta - \sinh\nu\sinh\tau , \tag{A14}$$

$$Y_{n1}(z) = (n+1)(n-2) B_{n-1,1,1,2}(z) - n(2n-1) z B_{n,1,1,2}(z) , \tag{A15}$$

$$Y_{n2}(z) = n(n+1)(n-2)\kappa^2 B_{n-1,0,0,1}(z) + (n-2)\kappa^2 z^2 B_{n-1,2,2,1}(z) \\ -2n(2n-1)[B_{n,1,1,2}(z) - \kappa^2 z^2 B_{n,1,2,1}(z)] , \tag{A16}$$

$$Y_{n3}(z) = n(n+1) B_{n,0,0,1}(z) - z^2 B_{n,2,2,1}(z) , \tag{A17}$$

$$Y_{n4}(z) = n(n+1) B_{n+1,0,0,1}(z) + z^2 B_{n+1,2,2,1}(z) , \tag{A18}$$

J_1 is the Bessel function of the first kind of order one, and the function $B_{n,m,j,l}(z)$ is defined by Equation (C5) of Ganatos et al. [13].

doi:10.6342/NTU202502370

A.2. Schematic representation of the defined parameters

To further clarify the meaning of the four dimensionless parameters (λb , b/d , $d/(d+c)$, and a/b) mentioned in Chapter 3, a supplementary diagram is provided in Figure A1. The diagram also illustrates the upper and lower limits of these parameters along with their corresponding geometric interpretations.

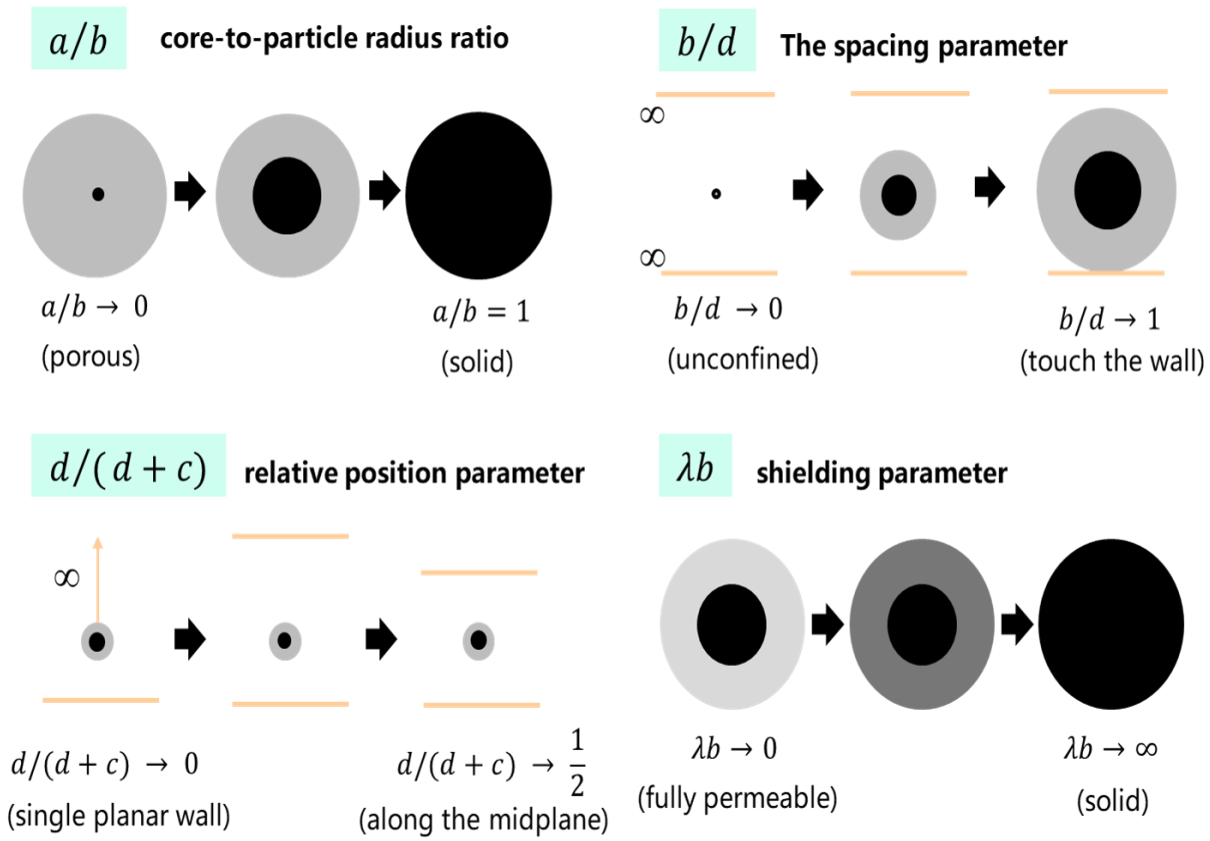

Figure A1. Geometric interpretation of the four parameters (λb , b/d , $d/(d+c)$, and a/b).

doi:10.6342/NTU202502370